MNRAS **000**, 1–10 (2018) Preprint 11 October 2021 Compiled using MNRAS LATEX style file v3.0

Testing tidal theory for evolved stars by using red-giant binaries observed by *Kepler*

P. G. Beck,[1,2] S. Mathis,[3,4,5] F. Gallet,[6] C. Charbonnel,[6,7]
M. Benbakoura,[3,4] R. A. García[3,4] & J.-D. do Nascimento, Jr.[8,9]

[1] *Instituto de Astrofísica de Canarias, E-38200 La Laguna, Tenerife, Spain*
[2] *Departamento de Astrofísica, Universidad de La Laguna, E-38206 La Laguna, Tenerife, Spain*
[3] *IRFU, CEA, Université Paris-Saclay, F-91191 Gif-sur-Yvette, France*
[4] *Université Paris Diderot, AIM, Sorbonne Paris Cité, CEA, CNRS, F-91191 Gif-sur-Yvette, France*
[5] *LESIA, Observatoire de Paris, PSL Research Univ., CNRS, Univ. Pierre et Marie Curie, Univ. Paris Diderot, 92195 Meudon, France*
[6] *Department of Astronomy, University of Geneva, Chemin des Maillettes 51, 1290, Versoix, Switzerland*
[7] *IRAP, UMR 5277, CNRS and Université de Toulouse, 14 Av. E. Belin, 31400, Toulouse, France*
[8] *Harvard-Smithsonian Center for Astrophysics, Cambridge, MA 02138, USA*
[9] *Departamento de Física, Universidade Federal do Rio Grande do Norte, CEP: 59072-970 Natal, RN, Brazil*

arXiv:1806.07208v1 [astro-ph.SR] 19 Jun 2018

submitted: 24 December 2017, accepted: 18 June 2018

ABSTRACT

Tidal interaction governs the redistribution of angular momentum in close binary stars and planetary systems and determines the systems evolution towards the possible equilibrium state. Turbulent friction acting on the equilibrium tide in the convective envelope of low-mass stars is known to have a strong impact on this exchange of angular momentum in binaries. Moreover, theoretical modelling in recent literature as well as presented in this paper suggests that the dissipation of the dynamical tide, constituted of tidal inertial waves propagating in the convective envelope, is weak compared to the dissipation of the equilibrium tide during the red-giant phase. This prediction is confirmed when we apply the equilibrium-tide formalism developed by Zahn (1977), Verbunt & Phinney (1995), and Remus, Mathis & Zahn (2012) onto the sample of all known red-giant binaries observed by the NASA *Kepler* mission. Moreover, the observations are adequately explained by only invoking the equilibrium tide dissipation. Such ensemble analysis also benefits from the seismic characterisation of the oscillating components and surface rotation rates. Through asteroseismology, previous claims of the eccentricity as an evolutionary state diagnostic are discarded. This result is important for our understanding of the evolution of multiple star and planetary systems during advanced stages of stellar evolution.

Key words: Stars: late-type, stars: binaries: spectroscopic, stars: oscillations, stars: kinematics and dynamics, stars: evolution, planet-star interactions

1 INTRODUCTION

A binary system has reached the state of minimum energy through tidal interactions when the orbit is circularised and the orbital and stellar spins are aligned and synchronised (e.g. Hut 1980; Zahn 2013). While for orbital periods shorter than ~10 days nearly all systems are circularised, a large spread in eccentricity is found for longer orbital periods (e.g. Mazeh 2008). Consequently, for wider binaries the orbital period alone is not sufficient to characterise tidal interactions (Verbunt & Phinney 1995, hereafter VP95; Torres et al. 2010). The efficiency of the physical processes that dissipate the kinetic and potential energies of tides into heat depends on stellar structure (in particular, the respective size and mass of the radiative and convection zones), fundamental parameters, and rotation. This determines the evolutionary pace for an eccentric binary towards equilibrium (e.g. Zahn 1977; Ogilvie & Lin 2007; Mathis 2015; Gallet et al. 2017).

In stars, tides can be understood as the combination of an equilibrium/non wave-like tide and of a dynamical/wave-like tide (e.g. Zahn 1977; Ogilvie 2013, 2014). The equilibrium tide is a large-scale flow driven by the hydrostatic adjustment of a star induced by the tidal gravitational perturbation due to the companion (e.g. Zahn 1966; Remus et al. 2012; Ogilvie 2013). It is efficiently dissipated in the convective envelope of low-mass stars during their evolution (e.g. Verbunt & Phinney 1995; Zahn & Bouchet 1989) because of the friction applied on its velocity field by turbulent convec-

© 2018 The Authors

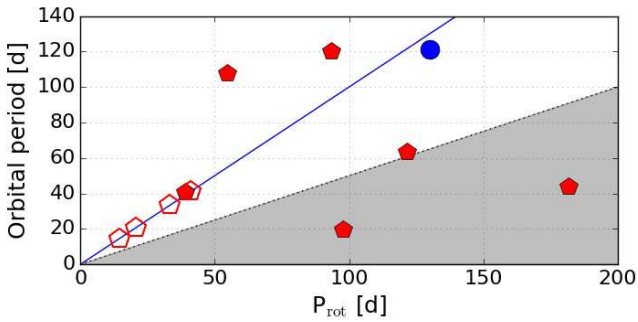


Figure 1. Orbital versus surface rotation period of *Kepler* red-giant binaries. The *grey* shaded area depicts the prohibited region for the dynamical tide, i.e., $P_{\rm orb} < \frac{1}{2} P_{\rm rot}$. Red pentagons and blue dots mark eclipsing (G14, G16) and heartbeat systems (B14, B18) observed by *Kepler*, respectively. Open symbols denote non-oscillating primaries.

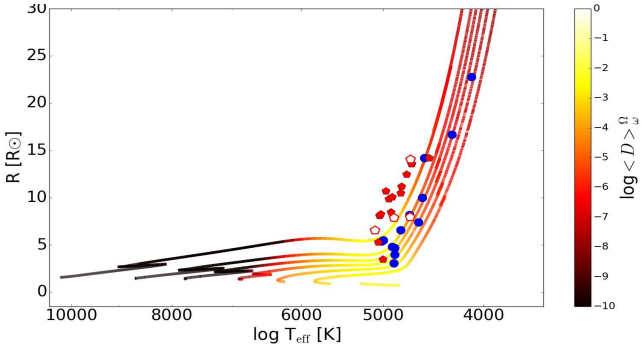


Figure 2. Dissipation of the dynamical tide as a function of stellar evolution. The colour-code reflects the intensity of the dissipation along the theoretical tracks starting at the zero-age main sequence in the R_*-$T_{\rm eff}$ plane, calculated for the sample mass range ($Z_\odot$ tracks for 0.8, 1.0, 1.2, 1.4, 1.6, 1.8, 2.0 & 2.2 $M_\odot$). The same symbols as in Fig. 1 are used.

tion (e.g. Zahn 1966; Mathis et al. 2016). However, the equilibrium tide is not a solution of the complete equations of stellar hydrodynamics and it must be completed by the so-called dynamical tide introduced by Zahn (1975). In rotating stars, it is constituted by tidal inertial waves that propagate in convective regions and are driven by the Coriolis acceleration (e.g. Ogilvie & Lin 2007; Ogilvie 2013; Mathis 2015) and by tidal gravito-inertial waves that are excited in stably stratified radiative zones and driven by buoyancy and the Coriolis acceleration (e.g. Zahn 1975; Terquem et al. 1998; Ogilvie & Lin 2007; Barker & Ogilvie 2010). They are damped by the convective turbulent friction and thermal diffusion and breaking, respectively.

Because of the long tidal evolution time scales compared to the existing time bases of observational data, such theoretical descriptions of tidal interactions within binary stars are difficult to probe empirically. VP95 however tested successfully their formalism for the dissipation of the equilibrium tide in evolving convective envelopes using a sample of spectroscopic red-giant binary systems located in open clusters. Today, this test can be extended, thanks to the NASA *Kepler* space mission, originally designed for detecting planetary transits (Borucki et al. 2010) which has been very successful in finding binary systems. Among the 197 100 stars observed by *Kepler* (Mathur et al. 2017), ~3000 binary stars are known (Kirk et al. 2016). Thirty-five of these systems contain a red-giant component. Through combination of space photometry, asteroseismology, and ground-based spectroscopy, these systems are well characterised (Frandsen et al. 2013, Gaulme et al. 2014, 2016, Rawls et al. 2016, Beck et al. 2014, 2018, hereafter F13, G14, G16, R16, B14, & B18). The main catalogs were presented by G14 & G16 and B14 (Tab. C1). While G14 & G16 focused on eclipsing systems, B14 presented binary stars exhibiting photometric signatures of tidal interactions due to the non-adiabatic component of the equilibrium tide, as predicted theoretically by Kumar et al. (1995). We refer to them as heartbeat stars, a term coined by Thompson et al. (2012).

In this work, we constrain the relative strength of the dissipation of the equilibrium and dynamical tides in red giant stars. We use the formalisms developed by VP95 and Remus et al. (2012) for the equilibrium tide as well as Ogilvie (2013) and Mathis (2015) for the dynamical tide and confront their predictions to the observed orbital properties of the *Kepler* red-giant binaries sample. We discuss tidal interactions in these systems in the light of surface rotation and seismology provided by *Kepler*.

2 TIDAL DISSIPATION IN RED GIANT STARS

2.1 Equilibrium tide

For stars with large convective envelopes such as red giant stars, the first of the main tidal dissipation mechanisms is the turbulent friction applied by convection on the equilibrium tide (e.g. Zahn 1966; Remus et al. 2012).

In the Appendix A, we provide the expression of this dissipation $\mathcal{D}_{\rm eq}$ as a function of the stellar structural properties and rotation and of the orbital period. It will be used to compare the respective strength of the equilibrium and dynamical tides on the RGB. In addition, we follow VP95 who rewrote the associated circularisation timescale $\tau_{\rm circ}$ derived by Zahn (1977) in the following way:

$$\frac{1}{\tau_{\rm circ}} = \frac{d\ln e}{dt} \simeq -1.7 f \cdot \left(\frac{T_{\rm eff}}{4500\,K}\right)^{4/3} \cdot \left(\frac{M_{\rm env}}{M_\odot}\right)^{2/3} \cdot \frac{M_\odot}{M_1} \cdot \frac{M_2}{M_1} \cdot \frac{M_1+M_2}{M_1} \cdot \left(\frac{R_1}{a}\right)^8 \quad [\mathrm{yr}^{-1}], \tag{1}$$

whereby the parameters of the primary and the secondary are the mass M and the radius R. The effective temperature and mass of the convective envelope of the giant component are given by $T_{\rm eff}$ and $M_{\rm env}$, respectively. The dimensionless parameter f is of the order of unity and determined by the details of the convective turbulent friction. Finally, a is the system's semi-major axis.

To quantify the tidal dissipation within the giant component in detached close binary systems and classify them, VP95 isolate the terms of Eq. (1) that depend on the parameters of the primary component and introduce the circularisation function

$$I(t) = \int_0^t \left(\frac{T_{\rm eff}}{4500\,K}\right)^{4/3} \cdot \left(\frac{M_{\rm env}(t')}{M_\odot}\right)^{2/3} \cdot \left(\frac{R_1(t')}{R_\odot}\right)^8 dt' . \tag{2}$$

By integrating Eq. (2) along the evolutionary tracks of representative stellar models, VP95 found that $I(t)$ is a monotonic function of the stellar radius that can be well approximated by the analytical expression

$$I = 7.6 \cdot 10^8 \cdot \left(\frac{R_1}{R_\odot}\right)^{6.51} \text{[yr]}\,. \quad (3)$$

For stars in the red-giant phase, the radius is the parameter that varies most drastically with time, more than two orders of magnitude, while the mass of the convective envelope and the effective temperature change only modestly. By using Eq. (1), Eq. (2), and Kepler's third law, VP95 derive the rate of eccentricity reduction,

$$\frac{\Delta \ln e}{f} = \frac{-1.7}{10^5} \cdot \left(\frac{M_1}{M_\odot}\right)^{-11/3} \cdot \frac{q}{(1+q)^{5/3}} \cdot I(t) \cdot \left(\frac{P_{\rm orb}}{\rm day}\right)^{-16/3} \quad (4)$$

with $q{=}M_2/M_1$ the components mass ratio. In their plots, VP95 use the logarithm of negative value of Eq. (4), which, for the convenience of the reader, we call in this work $\varepsilon_{\rm r}$.

$$\varepsilon_{\rm r} = \log\left[-\left(\frac{\Delta \ln e}{f}\right)\right]\,. \quad (5)$$

This quantity represents the inverse time scale of tidal circularisation as a diagnostic of the strength of the dissipation. We will compute it for our sample in Section 3.

2.2 Dynamical tide

In the deep convective envelope of red giant stars, the dynamical tide is constituted by tidal inertial waves driven by the Coriolis acceleration [1] if $P_{\rm orb} > \frac{1}{2}P_{\rm rot}$, with $P_{\rm orb}$ and $P_{\rm rot}$ the periods of the orbital motion and stellar surface rotation, respectively (Ogilvie & Lin 2007)[2]. As shown in Fig. 1, most of the eleven *Kepler* binary systems with known rotation periods (G14, G16, B14, B18, see Tab. C1) lie in the regime where tidal inertial waves can propagate.

We compute the structural frequency-averaged dissipation $<\mathcal{D}>_{\rm struct.}$ (see Eq. B4 and Eq. 3 in Gallet et al. 2017), introduced by Ogilvie (2013) and Mathis (2015) for standard (non-rotating) solar metallicity stellar models in the mass range $0.8 \leq {\rm M/M_\odot} \leq 2.2$ (covered by the sample of *Kepler* stars, see Tab. C1 in the Appendix) computed with the stellar evolution code STAREVOL (see Gallet et al. 2017, and references therein). As shown in Fig. 2, the dissipation varies *by* several orders of magnitude along the stellar evolution from the main-sequence to the Red Giant Branch (hereafter RGB) phase (see Ogilvie & Lin 2007, and Appendix B).

We see that for stars with solar-metallcity and masses above 1.4 $\rm M_\odot$ the structural frequency-averaged tidal dissipation is most efficient at the end of the sub-giant branch, while for stars with $0.8{\leq}{\rm M/M_\odot}{\leq}1.4$ it is efficient throughout the main-sequence and sub-giant branch. However the efficiency is reduced by several orders of magnitude, once the stars passed the bottom of the RGB. This diagram only shows the efficiency of dissipation due to the dynamical tide. From seismic analysis and comparison with the evolutionary tracks in the HRD it is shown that all our sample stars are on the RGB (see Sec. 4), with half of them lying in or just above the region of maximum dissipation.

On the their way towards the RGB, stars experience a rapid expansion of their convective envelope in mass to maintain a surface hydrostatic equilibrium. This results in a drastic reduction of the efficiency of the dissipation of tidal inertial waves because the stellar structure configuration tends towards a full-sphere configuration. Here the viscous friction acting on sheared inertial waves attractors become less efficient because inertial waves become regular (we refer to the detailed discussion in Mathis 2015). Simultaneously, the growing (in radius) envelope amplifies the strength of the dissipation of the equilibrium tide as shown by Eq. (A6).

3 COMPARISON WITH VP95 AND *Kepler* SAMPLES

VP95 applied their formalism to 28 well-studied binaries with giant components with masses derived from cluster isochrones. In Fig. 3, the orbital eccentricity e of the systems in the cluster-sample is plotted as a function of the orbital period and ε_r as black squares. While in the *e-P* plane no convincing structure is found, plotting the eccentricity versus ε_r separates efficiently the eccentric from the circularised systems. From their analysis, VP95 suggest that a value of $[\Delta \ln e/f] \simeq 3$ marks the approximate transition limit between quasi- and non-circularised systems. Following Eq. (5), we refer to this value as $\varepsilon_{\rm crit} \simeq 0.478$, which is marked as a vertical line in the right hand panel of Fig. 3. We note that $\varepsilon_{\rm crit}$ is not indicating an exact dichotomy between circularised and eccentric systems, but can be understood as the entry line to the rapid circularisation phase. Figure 3 suggests that $\varepsilon_{\rm crit}$ is lower for very eccentric systems.

The red-giant binaries found by the *Kepler* mission now provide a key comparison data set. The masses of the components are determined from seismology and dynamical approaches, complementing mass determination through isochrone fitting as done for the cluster stars. The literature parameters of the stars in the *Kepler* sample are given in Tab. C1. In the left panel of Fig. 3, eclipsing systems (F13, G14, G16) are depicted as red pentagons, while heartbeat stars (B14) are shown as blue dots.

From the full sample of *Kepler* red-giant binary systems, a subset of 19 stars were found by various studies to be double-lined spectroscopic binary (SB2) systems (F13, G16, R16, B18), providing us with precise mass ratios of the system. By comparing the seismic and the dynamical masses of the SB2, G16 showed that masses and radii derived from seismic scaling relations are overestimated by ~15% and 5%, respectively. Therefore, we use, whenever available, the dynamical or corrected seismically inferred masses. For 14 out of the 18 heartbeat stars, B14 reported orbital eccentricities, based on their spectroscopic radial velocity (RV) monitoring. For one heartbeat system, KIC 5006817, the mass ratio was constrained from a combined fit of the *Kepler* light and RV curve (B14). With the exception of KIC 913796 (B18), these systems have typically much fainter companions stars, making it observationally challenging to detect the secondary's spectrum. For the twelve remaining heartbeat systems with known seismic masses but unknown mass ratio, we assumed

[1] As a first step, we do not take into account the tidal dissipation in the radiative stellar core.
[2] In the case of eccentric systems, other tidal frequencies will be excited (see Appendix B and Zahn 1977; Ogilvie 2014).

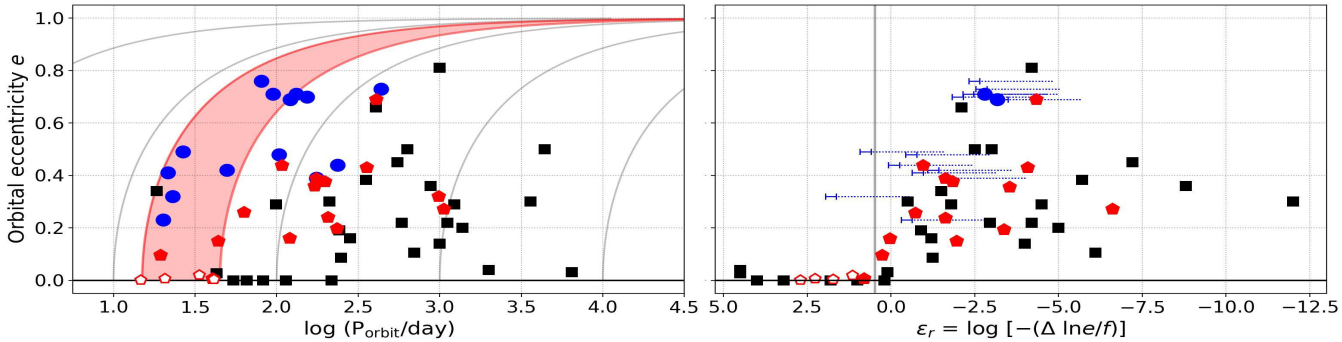


Figure 3. Eccentricity of red-giant binaries in the *Kepler* sample and open clusters. Red pentagons and blue dots mark *Kepler* red giants in eclipsing (G14, G16) and heartbeat systems (B14, B18), respectively. Open symbols denote non-oscillating primaries. The sample of VP95 cluster stars is shown as black squares. *Left:* e versus orbital period. Grey lines indicate tracks of constant angular momentum for circularised systems with periods of 10, 10^2, 10^3, and 10^4 days. The red shaded area marks the range of periods, $15 \leq P_{\rm circ} \leq 45$ days. *Right:* e versus the circularisation function ε_r. Following VP95, the horizontal axis is inverted. Filled symbols mark systems with known mass ratio, while blue solid 'H'-symbols indicate the ε_r-range, calculated for the mass ratio range, $1 \leq q \leq 1/5$, and blue dotted lines represent a mass ratio between unity and q≃1:1000. The vertical grey line depicts the value of $\varepsilon_{\rm crit}$.

a mass ratio $1/5 \leq q \leq 1$ (values taken from B18 and B14). To explore the expected range of ε_r for planetary systems, the mass ratio down to 1/1000 is depicted, representing an approximate mass ratio for a star hosting a giant planet. We note that in Fig. 2 systems from G16 are systematically hotter than those from B14. Such difference could overestimate the seismic masses and radii in G16 of a few percent but does not explain the full 15%.

The *Kepler* and the VP95-cluster samples are complementary in terms of primary mass and orbital periods, covered by each sample. With a mean primary mass of 2.0±0.4 $M_\odot$ the stars in the VP95 sample are substantially more massive than stars in the *Kepler* sample (1.3±0.3 $M_\odot$), but are very similar in terms of the mass ratio, 0.6±0.3 and 0.7±0.3, respectively. As shown in Fig. 3 (left panel), all except two systems of VP95 have orbital periods $P_{\rm orbit} \gtrsim 45$ d, and most eccentric systems are found at even periods of several hundred or thousand of days. Such long periodic systems are hard to detect from the ∼1400 d of *Kepler* photometry. The *Kepler* sample however contains systems with a wide range of eccentricities ($0 \leq e \lesssim 0.8$) at $P_{\rm orbit} \leq 45$ d. Combining both samples allows us to explore tides in short and long period systems. It is interesting to note that both samples are lacking systems with $0.5 \lesssim e \lesssim 0.7$. While the *Kepler* and cluster samples are different in their distribution in period (Fig. 3, left panel), viewing both samples in the e-ε_r plane leads to a very homogeneous pattern (right panel) with circularised systems (excepting KIC 2720096 and KIC 8095275) if $\varepsilon > \varepsilon_{\rm crit} \simeq 0.478$ (and eccentric ones if $\varepsilon < \varepsilon_{\rm crit}$). This shows that the VP95 formalism for the turbulent friction applied on the equilibrium tide in convective regions alone is sufficient to explain the observed time scales of circularisation of binary stars hosting giant-components and the corresponding eccentricity distribution. It is thus not necessary to invoke the action of the dynamical tide, which is predicted to be weak as demonstrated in Section 2.2 in the case of tidal inertial waves in RGB stars (see Fig. 2). A similar result is found for the planets (Fig. 3). Yet, the circularisation time scales are longer by several orders of magnitude (Fig. 3, right panel).

With KIC 2720096 (e=0.49, $P_{\rm orb}$=26.7 d) and KIC 8095275 (e=0.32, $P_{\rm orb}$=23.0 d) we find two eccentric heartbeat systems with $\varepsilon_{\rm r} \gg \varepsilon_{\rm crit}$ if a mass ratio $1/5 \leq q \leq 1$ is assumed. A lower value of q would place these systems closer or even below to $\varepsilon_{\rm crit}$. Comparing the power spectra of a synthetic and the observed light curve (following B18), indeed revealed no signature of the potential tidal inertial waves in the low-frequency regime. The VP95 formalism does not forbid such objects with $\varepsilon_{\rm r} \gg \varepsilon_{\rm crit}$, but because time scales for circularisation are short for such systems, we argue that they could be in a short lived phase of rapid circularisation during the evolution of some binary systems. We refer to them as 'forbidden binaries', in analogy to Kroupa (1995).

To investigate theoretically which tide dominates on the RGB, we define the quantity $\delta = \log(\mathcal{D}_{\rm eq}/<\mathcal{D}>_\omega)$ as the logarithm of the ratio between the dissipation of the equilibrium and the dynamical tide (Appendix A & B). Most stars with measured rotation periods originate from the G16 sample, in which the effective temperature and hence radius could be overestimated (see text above). To compensate for this complication in the estimate of the dissipation ratio, we computed the evolution of δ for each star with known $P_{\rm rot}$ along the RGB phase of our non-rotating stellar tracks (see Fig. 2). Using the 10^{th} percentile δ_{10} (i.e., the value below which 10% of the distribution may be found) of each δ evolution, we found that stars in the *Kepler* sample with known $P_{\rm rot}$, and regardless of the stellar mass, have 90% of chance to have at least a $\delta = 2.3$. This means that the equilibrium tide clearly dominates over the dynamical tide on the RGB and consequently also in the more advanced red-giant phases. Note that taking into account the effect of the stellar rotation on the effective turbulent friction (Mathis et al. 2016) significantly reduces $\mathcal{D}_{\rm eq}$ (see Strugarek et al. 2017) while still producing $\delta_{10} > 0$. Table C2 shows δ_{10} and the corresponding convective timescale $\tau_{\rm conv,10}$ (computed in the middle of the convective envelope) for the subsample of *Kepler* stars. In addition, most of the systems in our sample have a tidal period ($P_{\rm tide} \equiv 2\pi/\omega$), with ω the principal tidal frequency defined in Appendix A, longer than the possible range of convective turnover timescale computed from our stellar tracks. In these systems ($P_{\rm tide} \geq$ 12-14 d, $1.0 \lesssim M/M_\odot \lesssim 2.2$), the reduction factor for the eddy viscosity can thus be neglected.

4 SYNERGIES WITH SPACE PHOTOMETRY

The unparalleled quality of the photometric measurements collected by the *Kepler* mission allows for a discussion of the tidal interaction in the *Kepler* sample beyond the mere comparison with VP95. The detection of solar-like oscillations enables a thorough characterisation of the oscillating binary component (e.g. F13, G14, G16, B14, B18), as well as the detection of surface activity, modulated by rotation (as depicted in Fig. 1). Furthermore, asteroseismology of giant stars allows one to avoid systematic uncertainties, introduced by reddening corrections and the sample is not limited by the turn-off as it is the case for observations of cluster stars. By comparing surface rotation rates, derived from *Kepler* photometry (e.g. García et al. 2014; Ceillier et al. 2017) with the orbital periods, G14 associated short-period systems with mode depletion. When the surface rotation and orbital motion become synchronised in close binaries, the red-giant component could be spun up and the magnetic field generated by the dynamo (Privitera et al. 2016) can be responsible for the mode damping. Figure 3 shows that these four non-oscillating primaries are located in short period and quasi-circularised systems ($15 \leq P_{\rm orbit} \leq 45$ d and $e \leq 0.02$).

As for the orbital eccentricity, $\varepsilon_{\rm crit}$ serves as a proxy rather than a sharp cutoff between oscillating and non-oscillating systems, whereby the eccentricity plays an important role. Stars with no or suppressed oscillation amplitudes are all systems with $e \simeq 0$ at $\varepsilon_{\rm r} \gg \varepsilon_{\rm crit}$, as shown in the right hand panel of Fig. 3. This suggests that for quasi-circularised systems that $\varepsilon_{\rm crit}$ acts also as a limit between oscillating stars and stars with additional damping or complete suppression of oscillations. The only primary of a quasi-circularised system with detected oscillations is KIC 5308778 ($e \simeq 0.006$), which shows very small oscillation amplitudes, compared to compatible red-giant oscillators. With a difference of ~1.6 d between $P_{\rm orb}$ and $P_{\rm rot}$, KIC 5308778 (see Fig.1 Table C1) is indeed not yet fully spun up at the surface, which is the first layer to be synchronised with the orbital motion (e.g. Zahn 2013, and references therein), indicating that the deeper layers may be not synchronised as well. The forbidden binaries KIC 2720096 ($\varepsilon_{\rm r} \simeq 0.83$) and KIC 8095275 ($\varepsilon_{\rm r} \simeq 1.86$) are both oscillating. KIC 2720096 is showing depressed dipole modes with respect to the radial modes and exhibits the highest chromospheric activity found in the sample of B14. The oscillation amplitude of KIC 8095275 is normal. The tidal interaction affects the surface magnetism through the rotation-driven stellar dynamo. Since the surface magnetism is the responsible of the low amplitudes of the modes (e.g. G14, García et al. 2014), the connections with tidal interactions is thus an indirect one.

From their diagnostic diagrams (Fig. 5 in VP95), VP95 note that for primaries with radii between the maximum stellar radius at the tip of the RGB and the minimum radius in the red-clump (RC) phase, an ambiguity between evolutionary states exists. The high dependence of ε_r on the stellar radius (Eq. 3) suggests that H-shell burning stars, which are ascending the RGB should have been circularised when they reach the RC phase of quiescent He-core burning. Therefore, VP95 proposed the orbital eccentricity as a diagnostic to distinguish between the RGB and RC evolutionary stages, suggesting that circularised systems host RC stars. Based on the detection of mixed-dipole modes from high precision space photometry (Beck et al. 2011), asteroseismic techniques have been developed to discriminate between RGB and RC giants (e.g. Bedding et al. 2011; Kallinger et al. 2014). Applying such techniques, B14 found that all heartbeat systems in their sample are located on the RGB, while G14 found a mix of evolutionary states among their binaries. In a detailed reanalysis, Kallinger et al. (2018) found that all except one *oscillating* stars from G14 (KIC 9246715, e ~0.36, see also R16) belong to the less advanced RGB phase. This includes the only circularised oscillating system KIC 5308778.

With 14 $R_\odot$, KIC 4569590 could either be a RC star or a RGB star. On the other hand, the primary's radius from light curve models (G16) of the three other systems (~8 $R_\odot$) are only compatible with the stars belonging to the low-luminosity part of the RGB. To test if a more eccentric version of the system would have hosted a red-giant star at the tip of the RGB, we calculated tracks of constant angular momentum in the $P_{\rm orbit}$-e plane (Mazeh 2008) for a system with a circular orbit periods, $P_{\rm circ}$,

$$P_{\rm circ} = P\left(1 - e^2\right)^{3/2} . \quad (6)$$

The possible area for eccentric versions of the now-circularised *Kepler* stars in this diagram is shown as red surface in the left hand panel of Fig. 3. We note that the track for $P_{\rm circ} = 15$ d describes the outer envelope for the distribution of binaries. Therefore, a progenitor system with $e \simeq 0.7$ would have had a period of about 100 days. Given the close separation at periastron, such system will eventually undergo a common envelope phase on the low-luminosity RGB (B14). Therefore, the orbital eccentricity cannot serve as a diagnostic of the evolutionary state for stars.

5 CONCLUSIONS

We tested the theory of tidal interaction on binary systems that host a red-giant component and are well characterised through *Kepler* photometry. We found that the action of the turbulent friction acting on the equilibrium tide in the deep convective envelope of RGB stars allows us to understand the eccentricity-period distribution. Dissipation of tidal inertial waves is thus not required to explain the observed eccentricities in the analysed sample of stars. From our calculations, based on models of Remus et al. (2012) and Gallet et al. (2017), we show that this component of the dynamical tide is expected to be weak when compared to the equilibrium tide. This is confirmed by the lack of observational signatures (B18). Therefore, the dynamical tide has a negligible contribution to the tidal dissipation budget in evolved stars with large convective envelopes

This study benefits from complementary observational constraints, provided by the *Kepler* satellite. Therefore, we could extend the discussion of ε_r beyond eccentricity and use the presence of stellar oscillation. Knowing the surface rotation, allows us to test for synchronisation of the primary with orbital motion. From this approach, we suggest that the previously reported mode depletion is connected indirectly, via a rotation-driven dynamo, to strong tidal interactions on short circularisation time scales ($\varepsilon_r > \varepsilon_{\rm crit}$). Consequently, the control physical parameter is the volume of the convective envelope of the giant component. Using asteroseismic

constraints, we showed that eccentricity cannot serve as a diagnostic for the evolutionary state of the primary.

ACKNOWLEDGEMENTS

We thank the referee for useful comments that allowed us to improve the article. PGB acknowledges support by the MINECO-prog.'Juan de la Cierva Incorporacion' (IJCI-2015-26034). RAG acknowledges the ANR, France, prog. IDEE (n°ANR-12-BS05-0008). StM acknowledges the ERC through SPIRE (grant No. 647383). RAG and StM acknowledge support from CNES PLATO grant at CEA. FG acknowledges support from the CNES fellowship. FG & CC acknowledge support from the Swiss National Science Foundation & SEFRI for proj. C.140049 under COST Action TD 1308 Origins.

REFERENCES

Barker A. J., Ogilvie G. I., 2010, MNRAS, 404, 1849
Beck P. G., et al., 2011, Science, 332, 205
Beck P. G., et al., 2014, A&A, 564, A36
Beck P. G., et al., 2018, A&A, 612, A22
Bedding T. R., et al., 2011, Nature, 471, 608
Borucki W. J., et al., 2010, Science, 327, 977
Brun A. S., García R. A., Houdek G., Nandy D., Pinsonneault M., 2015, Space Sci. Rev., 196, 303
Ceillier T., et al., 2017, A&A, 605, A111
Di Mauro M. P., et al., 2016, ApJ, 817, 65
Frandsen S., et al., 2013, A&A, 556, A138
Gallet F., et al., 2017, A&A, 604, A112
García R. A., et al., 2014, A&A, 572, A34
Gaulme P., Jackiewicz J., Appourchaux T., Mosser B., 2014, ApJ, 785, 5
Gaulme P., et al., 2016, ApJ, 832, 121
Hut P., 1980, A&A, 92, 167
Kallinger T., et al., 2014, A&A, 570, A41
Kallinger T., et al., 2018, preprint, (arXiv:1805.06249)
Kirk B., et al., 2016, AJ, 151, 68
Kroupa P., 1995, MNRAS, 277
Kumar P., Ao C. O., Quataert E. J., 1995, ApJ, 449, 294
Mathis S., 2015, A&A, 580, L3
Mathis S., et al., 2016, A&A, 592, A33
Mathur S., et al., 2017, ApJS, 229, 30
Mazeh T., 2008, in EAS Pub. Series. (arXiv:0801.0134)
Ogilvie G. I., 2013, MNRAS, 429, 613
Ogilvie G. I., 2014, ARA&A, 52, 171
Ogilvie G. I., Lin D. N. C., 2007, ApJ, 661, 1180
Privitera G., et al., 2016, A&A, 593, L15
Rawls M. L., et al., 2016, ApJ, 818, 108
Remus F., Mathis S., Zahn J.-P., 2012, A&A, 544, A132
Strugarek A., et al., 2017, ApJ, 847, L16
Terquem C., et al., 1998, ApJ, 502, 788
Thompson S. E., et al., 2012, ApJ, 753, 86
Torres G., Andersen J., Giménez A., 2010, A&Ar, 18, 67
Verbunt F., Phinney E. S., 1995, A&A, 296, 709
Zahn J. P., 1966, Annales d'Astrophysique, 29, 489
Zahn J.-P., 1975, A&A, 41, 329
Zahn J.-P., 1977, A&A, 57, 383
Zahn J.-P., 2013, in Lecture Notes in Physics, Vol. 861, 301.
Zahn J.-P., Bouchet L., 1989, A&A, 223, 112

APPENDIX A: EFFICIENCY OF THE EQUILIBRIUM TIDE DISSIPATION

The dissipation of the equilibrium tide can be estimated using the theoretical model developed by Remus et al. (2012). They obtained

$$\mathcal{D}_{\rm eq} = 4\pi \frac{2088}{35} \frac{R_\star^4}{GM_\star^2} \left| \omega \int_\alpha^1 x^8 \rho \nu_t \, {\rm d}x \right|, \tag{A1}$$

where ω is the tidal frequency, which is evaluated here using $\omega = 2\,(\Omega_{\rm orb} - \Omega_\star)$ the principal tidal frequency with $\Omega_{\rm orb} = 2\pi/P_{\rm orb}$ the orbital frequency of the companion and $\Omega_\star = 2\pi/P_{\rm rot}$ the stellar surface rotation frequency. We introduced G the gravitational constant, ν_t the effective turbulent viscosity applied on tides in the convective zone, $\alpha = R_{\rm c}/R_\star$, $R_{\rm c}$ being the radius of its base and $R_\star$ the radius of the star, ρ the density in the convection zone, and $x = r/R_\star$ the normalised radial coordinate.

We derive hereafter an estimate of Eq. (A1) as a function of the global parameters of the system.

The turbulent viscosity strength depends on how the convective turnover time $\tau_{\rm conv}$ compares to the tidal frequency ω. We here follow Remus et al. (2012) and we get

$$\nu_t = \frac{1}{3} v_{\rm conv} l_{\rm conv} \left[1 + \left(\frac{\tau_{\rm conv} \omega}{\pi} \right)^2 \right]^{-1/2}, \tag{A2}$$

where v_c is the typical convective velocity and l_c the mixing length. We here assume the linear attenuation of the effective turbulent friction applied on tides for short tidal period ($P_{\rm tide} = 2\pi/\omega$) as proposed by Zahn (1966). In the case where we neglect the action of rotation on the effective turbulent friction applied to the equilibrium tide (Mathis et al. 2016) because we compute here non-rotating stellar models, we can write (e.g. Brun et al. 2015)

$$v_{\rm conv} \simeq \left(\frac{L_\star}{\rho_{\rm c} R_\star^2} \right)^{1/3}, \tag{A3}$$

$$l_{\rm conv} \simeq \alpha_{\rm MLT} H_P, \tag{A4}$$

$$\tau_{\rm conv} = \frac{l_{\rm conv}}{v_{\rm conv}}, \tag{A5}$$

where we have introduced the stellar luminosity $L_\star$, the average density in the convection zone $\rho_{\rm c}$, the mixing-length parameter $\alpha_{\rm MLT}$, and the pressure scale height H_P. To provide an order of magnitude of the dissipation as a function of stellar global parameters, we assume the simplest approximations that $\rho = \rho_{\rm c}$ and that ν_t in the integral in Eq. (A1) does not vary with depth. In addition, we approximate the mixing length l_c by its maximum which is given by the depth of the convection zone $(1-\alpha)R_\star$. Finally, we express the mean density of the convective envelope as a function of the mass ratio $\beta = M_{\rm c}/M_\star$, where $M_{\rm c}$ is the radiative core mass. We get $\rho_{\rm c} = 3M_\star\,(1-\beta)\,/4\pi R_\star^3 \left(1-\alpha^3\right)$ that leads to

$$\mathcal{D}_{\rm eq} \simeq \frac{232}{35} \frac{|\tau_{\rm conv}\,\omega|}{\sqrt{1 + \left(\frac{\tau_{\rm conv}\,\omega}{\pi} \right)^2}} \frac{R_\star}{GM_\star} v_{\rm conv}^2 (1-\beta) \frac{1-\alpha^9}{1-\alpha^3}. \tag{A6}$$

APPENDIX B: FREQUENCY-AVERAGED DISSIPATION OF THE DYNAMICAL TIDE

In the formalism of Ogilvie (2013) and Mathis (2015), the stellar convective envelope is assumed to be in solid-body rotation with a uniform angular velocity $\Omega_\star$. The assumption of such flat rotation profile in the envelope is supported by observational and theoretical studies of the rotation profile in the convective envelope of RGB stars (Beck et al. 2018; Di Mauro et al. 2016, respectively). Moderate rotation is assumed, i.e., the squared ratio of $\Omega_\star$ to the critical angular velocity $\Omega_{\rm crit}$ is such that

$$(\Omega_\star/\Omega_{\rm crit})^2 = \left(\frac{\Omega_\star}{\sqrt{\mathcal{G}M_\star/R_\star^3}}\right)^2 \equiv \epsilon^2 < 1\,. \tag{B1}$$

The effects of the centrifugal acceleration are thus neglected. We use two-layer models following Ogilvie (2013) and Mathis (2015) to evaluate the frequency-averaged tidal inertial waves dissipation in the stellar convective envelope and we focus on solar-metallicity stars with initial masses between 0.3 and 1.4 $M_\odot$. In this mass range, the convective envelope surrounds the radiative core of radius $R_{\rm c}$ and mass $M_{\rm c}$. In our two-layer model, both core and envelope are assumed to be homogeneous with respective average densities $\rho_{\rm c}$ and $\rho_{\rm e}$. This allows an analytical treatment of the problem. Such a two-layer model is commonly used in the representative forward-modelling approach in asteroseismology. Recent theoretical and observational results by Di Mauro et al. (2016) and Beck et al. (2018), respectively, have confirmed that this simplification can be used.

In the case of a coplanar binary system in which the orbit of the planet is circular, this frequency-averaged tidal dissipation is given by (see Eq. B4 from Ogilvie 2013),

$$< \mathcal{D} >_\omega = \int_{-\infty}^{+\infty} {\rm Im}\left[{\rm k}_2^2(\omega)\right]\frac{{\rm d}\omega}{\omega} = \frac{100\pi}{63}\epsilon^2\left(\frac{\alpha^5}{1-\alpha^5}\right)(1-\gamma)^2 \tag{B2}$$
$$\times(1-\alpha)^4\left(1+2\alpha+3\alpha^3+\frac{3}{2}\alpha^3\right)^2\left[1+\left(\frac{1-\gamma}{\gamma}\right)\alpha^3\right]$$
$$\times\left[1+\frac{3}{2}\gamma+\frac{5}{2\gamma}\left(1+\frac{1}{2}\gamma-\frac{3}{2}\gamma^2\right)\alpha^3-\frac{9}{4}(1-\gamma)\,\alpha^5\right]^{-2},$$

with

$$\gamma = \frac{\rho_{\rm e}}{\rho_{\rm c}} = \frac{\alpha^3(1-\beta)}{\beta(1-\alpha^3)} < 1. \tag{B3}$$

As in Mathis (2015), we can express a structural frequency-averaged dissipation:

$$< \mathcal{D} >_{\rm struct.} = \epsilon^{-2} < \mathcal{D} > = \epsilon^{-2} < {\rm Im}\left[{\rm k}_2^2(\omega)\right] >_\omega, \tag{B4}$$

that only depends on α and β.

We know that tidal inertial waves dissipation can vary over several orders of magnitude as a function of the forcing frequency (Ogilvie & Lin 2007). As discussed in Mathis (2015), the frequency-averaged dissipation thus provides us a qualitative order of magnitude of this dissipation for a rotating star at a given evolutionary stage.

We note that here we use prescriptions for the dynamical tide derived for a coplanar and circular system. In this simplified case, the tidal frequency is the principal one given by $\omega = 2\,(\Omega_{\rm orb} - \Omega_\star)$. Moreover, in that configuration the tidal potential is described by the spherical harmonic of degree l=2, m=±2 and thus by the love number k_2^2. Taking into account coherently the eccentricity will require to consider general tidal frequencies $\omega = L\Omega_{\rm orb} - m\Omega_\star$ (where L is an integer number) that include the principal tidal frequency for which $L = 2$ and $m = 2$, and other spherical harmonic components of the tidal potential and corresponding complex Love numbers $\left(k_2^0\right)$ (Zahn 1977; Ogilvie 2014).

APPENDIX C: LITERATURE VALUES FOR *Kepler*-SYSTEMS

The parameters for eclipsing binaries are taken from the dynamical solution of G16. For the list of heartbeat stars (B14), radius and mass were inferred from seismic scaling relations and corrected for the systematic mass overestimate of 15% reported by G16. Surface rotation periods were adopted from G14, B14 and B18. For four stars of B14, KIC 7431665, KIC 11044668, KIC 8803882, and KIC 7799540, no orbital parameters have yet been published.

C1 Content of Table C1

We refer to the cited literature for details on the applied methodology. Table C1 contains the following parameters,

- *KIC* specifies the target identification number in the *Kepler* Input Catalog.
- *Type* indicates if a binary system is an eclipsing binary (EB), a heartbeat system (HB), or an eclipsing heartbeat system (eHB). 'NO' indicates that the star belongs to the four non-oscillating stars of G14/G16.
- $\rm P_{orbit}$ is the measured orbital period.
- e is the orbital eccentricity.
- $\nu_{\rm max}$ is the peak frequency of the excess of oscillation power.
- $R/R_\odot$ is the stellar radius in solar units. Values from B14 are seismically inferred and corrected for the 5% overestimate of seismic radius. Values from G16 originate from a dynamical solution.
- $M/M_\odot$ is the stellar mass in solar units. Values from B14 are seismically inferred and corrected for the 15% overestimate of seismic mass. Values from G16 originate from a dynamical solution.
- $q = M_2/M_1$ is the mass ratio between the two stellar components in the system. '?' indicates if q has not been determined for a given system.
- $T_{\rm eff}$ is the effective temperature.
- $P_{\rm rot}$ specifies the time scale of the flux modulation, identified as the surface rotation period. The sources of the values are G14 and B18. We round all period values to the next full day.
- The dimensionless number ε_r is proportional to the inverse of the time scale of tidal circularisation (see Eq. 5). If no value of the mass ratio is specified, ε_r is calculated for $q = 0.5$.
- REF: the last column is specifying the literature references. If several papers are reporting on a given system, values of the most recent paper are cited. Previous references are given in brackets.

C2 Content of Table C2

Table C2 lists the following parameters for the systems' red-giant primary with known $P_{\rm rot}$,

- δ_{10} is the $10^{\rm th}$ percentile of the logarithm of the ratio between the dissipation of the equilibrium and the dynamical tide, $\delta = \log(\mathcal{D}_{\rm eq} / <\mathcal{D}>_{\omega})$.
- $\tau_{\rm conv,10}$ is the corresponding convective turnover timescale computed in the middle of the convective zone.
- $P_{\rm tide} > \tau_{\rm conv,10}$ indicates if the tidal period is longer than the convective turnover timescale (Yes / No).

Table C2. Evolution of δ_{10} for the systems with know rotation period.

KIC	$P_{\rm tide}$ [days]	$\tau_{\rm conv,10}$ [days]	$P_{\rm tide} > \tau_{\rm conv,10}$	δ_{10}
7943602	357	20	Y	2.3-3.4
7377422	56	20	Y	3.7-4.8
3955867	845	20-23	Y	2.6-3.7
9291629	692	20-23	Y	2.3-3.4
5179609	28	23	Y	4.7-5.8
9163796	906	23	Y	3.8-4.9
8430105	65	23-26	Y	4.4-5.5
5308778	505	12	Y	3.0-4.1
4569590	2285	12	Y	2.4-3.5
8702921	12	12	N	4.2-5.3
9246715	101	14	Y	4.1-5.2

Table C1. Literature Parameters of red-giant binaries in the *Kepler* sample.

KIC	Type	P_{orb} [days]	e []	ν_{max} [μHz]	$R/R_\odot$ []	$M/M_\odot$ []	q []	T [K]	P_{rot} [days]	ε_r []	REF
2444348	HB	103.50 ± 0.01	0.48 ± 0.01	30.5 ± 0.3	14.2 ± 0.3	1.6 ± 0.1	?	4565	-	-0.53	B14
2697935	eHB	21.50 ± 0.02	0.41 ± 0.02	~ 405.6	~ 3.1	~ 1.2	?	4883	-	-0.73	B14
2720096	HB	26.70 ± 0.01	0.49 ± 0.01	110.1 ± 0.7	6.6 ± 0.1	1.3 ± 0.1	?	4812	-	0.83	B14
3955867	EB, NO	33.65685 ± 0.00007	0.019 ± 0.002	–	7.9 ± 0.1	1.10 ± 0.06	0.84 ± 0.05	4884	33	1.14	G16 (G14)
4569590	EB, NO	41.3710 ± 0.0001	0.004 ± 0.001	–	14.1 ± 0.2	1.6 ± 0.10	0.66 ± 0.05	4706	41	1.67	G16 (G14)
4663623	EB	358.09 ± 0.0003	0.43 ± 0.01	54.1 ± 0.2	9.7 ± 0.2	1.36 ± 0.09	0.99 ± 0.08	4812	-	-4.08	G16 (G14)
5006817	HB	94.812 ± 0.002	0.71 ± 0.01	145.9 ± 0.5	5.5 ± 0.1	1.3 ± 0.1	0.199 ± 0.001	5000	-	-2.80	B14
5039392	HB	236.70 ± 0.02	0.44 ± 0.01	6.2 ± 0.1	22.8 ± 0.7	0.8 ± 0.1	?	4110	-	-0.01	B14
5179609	EB	43.93108 ± 0.000002	0.150 ± 0.001	322 ± 1.0	3.50 ± 0.03	1.18 ± 0.03	0.51 ± 0.02	5003	182	-1.96	G16 (G14)
5308778	EB	40.5661 ± 0.0003	0.006 ± 0.005	49 ± 1.1	10.1 ± 0.3	1.5 ± 0.1	0.43 ± 0.03	4900	39	0.80	G16 (G14)
5786154	EB	197.918 ± 0.0004	0.3764 ± 0.0009	29.8 ± 0.2	11.4 ± 0.2	1.06 ± 0.06	0.96 ± 0.07	4747	-	-1.85	G16 (G14)
7037405	EB	207.1083 ± 0.0007	0.238 ± 0.004	21.8 ± 0.1	14.1 ± 0.2	1.25 ± 0.04	0.91 ± 0.03	4516	-	-1.62	G16 (G14)
7377422	EB	107.6213 ± 0.0004	0.4377 ± 0.0005	40 ± 2.1	9.5 ± 0.2	1.05 ± 0.08	0.81 ± 0.07	4938	55	-0.96	G16 (G14)
7943602	EB, NO	14.69199 ± 0.00004	0.001 ± 0.003	–	6.6 ± 0.2	1.0 ± 0.10	0.78 ± 0.09	5096	15	2.70	G16 (G14)
8054233	EB	1058.16 ± 0.02	0.2718 ± 0.0004	46.5 ± 0.3	10.7 ± 0.1	1.60 ± 0.06	0.69 ± 0.04	4971	-	-6.61	G16 (G14)
8095275	HB	23.00 ± 0.01	0.32 ± 0.01	69.3 ± 0.3	7.4 ± 0.1	1.0 ± 0.1	?	4622	-	1.86	B14
8144355	HB	80.55 ± 0.01	0.76 ± 0.01	179.0 ± 2	4.7 ± 0.1	1.1 ± 0.1	?	4875	-	-2.41	B14
8210370	HB	153.50 ± 0.01	0.70 ± 0.01	44.1 ± 0.8	10.0 ± 0.2	1.2 ± 0.1	?	4585	-	-1.92	B14
8410637	EB	408.3 ± 0.5	0.689 ± 0.001	46.0 ± 0.2	10.7 ± 0.1	1.56 ± 0.3	0.85 ± 0.16	4800	-	-4.34	F13
8430105	EB	63.32713 ± 0.00003	0.2564 ± 0.0002	76.7 ± 0.6	7.65 ± 0.05	1.31 ± 0.02	0.63 ± 0.01	5042	122	-0.73	G16 (G14)
8702921	EB	19.38446 ± 0.00002	0.0964 ± 0.0008	195.6 ± 0.5	5.32 ± 0.05	1.67 ± 0.05	0.16 ± 0.01	5058	98	0.26	G16 (G14)
8912308	HB	20.17 ± 0.01	0.23 ± 0.01	~ 350.0 0	~ 4.0	~ 1.7	?	4872	-	-0.39	B14
9151763	HB	437.51 ± 0.03	0.73 ± 0.01	13.8 ± 0.2	16.7 ± 0.4	1.0 ± 0.1	?	4290	-	-2.62	B14
9163796	HB	121.30 ± 0.01	0.69 ± 0.002	165.3 ± 1.3	5.1 ± 0.1	1.2 ± 0.1	0.985 ± 0.005	4960	130	-3.17	B18 (B14)
9246715	EB	171.27688 ± 0.00001	0.3559 ± 0.0003	106.4 ± 0.8	8.30 ± 0.04	2.149 ± 0.007	0.990 ± 0.005	5030	93	-3.54	R16 (G14)
9291629	EB, NO	20.68643 ± 0.00004	0.007 ± 0.002	–	7.99 ± 0.05	1.14 ± 0.03	0.96 ± 0.03	4713	21	2.26	G16 (G14)
9408183	HB	49.70 ± 0.01	0.42 ± 0.01	164.8 ± 0.2	4.8 ± 0.1	1.0 ± 0.1	?	4900	-	-1.18	B14
9540226	eHB	175.4439 ± 0.0006	0.3880 ± 0.0002	27.1 ± 0.2	12.8 ± 0.1	1.33 ± 0.05	0.74 ± 0.04	4692	-	-1.64	G16 (B14, G14)
9970396	EB	235.2985 ± 0.0002	0.194 ± 0.007	63.7 ± 0.2	8.0 ± 0.2	1.14 ± 0.03	0.89 ± 0.03	4916	-	-3.38	G16 (G14)
10001167	EB	120.3903 ± 0.0005	0.159 ± 0.003	19.9 ± 0.1	12.7 ± 0.3	0.81 ± 0.05	0.98 ± 0.07	4700	-	0.03	G16 (G14)
10614012	eHB	132.13 ± 0.01	0.71 ± 0.01	70.2 ± 0.9	8.2 ± 0.2	1.3 ± 0.1	?	4715	-	-2.23	B14

This paper has been typeset from a TEX/LATEX file prepared by the author.